Hindawi
International Journal of Energy Research
Volume 2023, Article ID 2831961, 10 pages
https://doi.org/10.1155/2023/2831961

Research Article

Electronic, Thermal, and Thermoelectric Transport Properties of $ReSe_2$ and Re_2Te_5

Joonho Bang,[1,2] Okmin Park,[3] Hyun-Sik Kim,[3] Seung-Mee Hwang,[3] Se Woong Lee,[3] Sang Jeoung Park,[3] and Sang-il Kim[3]

[1]*School of Materials Science and Engineering, Gyeongsang National University, Jinju 52828, Republic of Korea*
[2]*Department of Materials Engineering and Convergence Technology, Gyeongsang National University, Jinju 52828, Republic of Korea*
[3]*Department of Materials Science and Engineering, University of Seoul, Seoul 02504, Republic of Korea*

Correspondence should be addressed to Sang-il Kim; sang1.kim@uos.ac.kr

Received 26 September 2022; Revised 2 November 2022; Accepted 3 November 2022; Published 6 February 2023

Academic Editor: Tholkappiyan Ramachandran

Re-based chalcogenides have been studied in various fields such as strain engineering, photodetection, spintronics, and electromechanics, as well as in piezoelectric and photonic devices. In this study, the electrical, thermal, and thermoelectric transport properties of two representative Re-based chalcogenides, $ReSe_2$ and Re_2Te_5, are investigated systematically. Furthermore, their electronic band dispersions are calculated using density functional theory and compared with the phenomenological data. The maximum power factor values for the $ReSe_2$ and Re_2Te_5 were measured 0.0066 and 0.11 mW/mK^2 at 880 K, respectively. Thermal conductivity of layered $ReSe_2$ at room temperature was between 1.93 and 8.73 W/mK according to the measuring direction. For Re_2Te_5 with a complex orthorhombic crystal structure, the thermal conductivity was quite low in the range between 0.62 and 1.23 W/mK at room temperature. As a result, the maximum zT values of $ReSe_2$ were quite low as 0.0016 at 880 K due to very low power factor and high thermal conductivity. Meanwhile, the relatively high zT of 0.145 in Re_2Te_5 is obtained at 880 K, which is originated from the acceptable power factor value and the low thermal conductivity.

1. Introduction

Metal chalcogenides have been receiving increasing attention as potential energy materials due to their tunable electronic properties and unique crystal structures, as well as relatively higher electrical conductivity in comparison to their transition metal oxide counterparts [1–3]. In particular, semiconductor chalcogenides have been widely used in thermoelectric (TE) fields because they have high electrical conductivity and low thermal conductivity, or even due to their unique crystal structures [4–6]. Among them, the layered structure that occupies most of the chalcogenides secures low thermal conductivity due to weak layer-to-layer van der Waals bonding. This is a key point because TE materials' performance is evaluated using a dimensionless thermoelectric figure of merit, $zT = S^2\sigma T/\kappa$ (where S, σ, κ, and T are the Seebeck coefficient, electrical conductivity, thermal conductivity, and absolute temperature, respectively). Therefore, several studies on layered chalcogenides are still being conducted to search for new thermoelectric materials. In fact, layered chalcogenides such as Bi-Te-based materials, InSe, In_4Se_3, $HfTe_2$, and $SnSe_2$ are famous TE materials that have high σ and low κ [7–13]. Bi-Te-based materials with high zT at 300-400 K have been reported in various studies [7–9]. In_4Se_3 was reported to have a zT value of 1.48 at 705 K [11].

Transition metal chalcogenides (TMCs), which have mostly layered structures, are also applicable in the same context. Recently, TMCs have been applied to a wide range of applications including nanoelectronics, sensors, energy conversion, and energy storage as 2D materials [14]. In addition, among the layered TMCs, chalcogenide materials that are based on Zr, Ti, W, and Mo have been widely used in the TE field [15, 16].

$ReSe_2$ is a one-layered TMC and has been studied in various fields such as strain engineering, photodetection, spintronics, and electromechanics, as well as in piezoelectric and photonic devices [17–20]. In addition, $ReSe_2$ is semiconductor that has a distinct band gap (1.26 eV for bulk $ReSe_2$) according to the density functional theory (DFT) of generalized gradient approximation (GGA) calculations from Hafeez et al. and Wolverson et al. [21, 22]. Thus, $ReSe_2$ may exhibit good TE properties and could be more advantageous due to the interlayer distance being 0.7 nm longer than other layered TMCs such as MoS_2 and WS_2 [17, 23], which leads to lower κ. Since the interlayer distance is long, κ of $ReSe_2$ can be predicted to being substantially large between the *ab*- and *c*-axes. Mahmoud and Joubert calculated lattice thermal conductivity (κ_{latt}) based on bulk $ReSe_2$ through first principles. In their study, κ_{latt} of the (100) and (010) directions were 18.47 and 17.44 W/mK at 300 K, respectively. However, κ_{latt} of the (001) direction was 0.69 W/mK [24]. If these characteristics are used well, $ReSe_2$ can be judged to having sufficient potential as a TE material.

Re_2Te_5, which is another rhenium chalcogenide semiconductor, is not a layered TMC but has a complex orthorhombic crystal structure with 84 atoms ($[Re_{24}]$ and $[Te_{60}]$) per unit cell. These atoms exhibit a cluster-type Chevrel phase with $[Re_6]$ surrounded by $[Te_8]$ [25–27]. One notable structural property of the Chevrel phase is the presence of 4 large vacancies. This causes the scattering of phonons, which effectively reduces κ_{latt}. Because of this, κ of Re_2Te_5 is 1.3 W/mK, which is similar to that of layered TMCs [28, 29]. In addition, it has the merit of being able to enhance thermoelectric properties through various doping in the 4 vacancies. In fact, Caillat et al. reported that rattling was found in elements doped into the vacancies, resulting in reduced κ due to phonon scattering [30].

In this study, the electrical, thermal, and thermoelectric transport properties of $ReSe_2$ and Re_2Te_5 samples were investigated. Notably, the electrical transport properties of $ReSe_2$ and Re_2Te_5 can be analyzed in more detail using a single parabolic band model. Based on this, the density-of-state effective mass, m_d^*, was calculated, and zT was evaluated to confirm the thermoelectric performances. In addition, the measured electrical transport properties were compared with calculated from first-principle DFT calculations.

2. Experimental Method

The $ReSe_2$ and Re_2Te_5 samples were synthesized via a conventional solid-state reaction process in a vacuum-sealed quartz tube. High-purity elements Te (99.999%), Se (99.999%), and Re (99.99%) powders were weighed with stoichiometric compositions, and mixed powder was loaded in the vacuum-sealed quartz tube. The loaded quartz ampoules were then heated to 950°C for 6 h and this temperature was maintained for 70 h. The synthesized $ReSe_2$ and Re_2Te_5 were pulverized into powders through high-energy ball milling (SPEX 8000D, SPEX) in Ar atmosphere. The $ReSe_2$ and Re_2Te_5 powders were placed into a graphite mold and pressed for sintering by spark plasma sintering (SPS, SPS-1030, Sumitomo Coal Mining Co., Ltd.). The $ReSe_2$ and Re_2Te_5 loaded into graphite molds were sintered at 950°C for 20 min under 70 MPa and 850°C for 10 min under 70 MPa, respectively. During the sintering, vacuum was maintained in the inside of the SPS chamber (~10^{-5} Torr).

The crystalline phases of the samples were identified using powder X-ray diffraction (XRD) with a Bruker D8 Discover (Cu K_α, $\lambda = 1.54059$ Å) diffractometer at room temperature. XRD measurements for the sintered pellet samples were carried out in two different directions, perpendicular ($\perp$) and parallel ($\parallel$) directions to the SPS pressing direction. The thermoelectric transport properties (σ and S) were measured simultaneously using a thermoelectric-property measurement system (ZEM-3, Advanced-Riko) in the two different directions within a temperature range of 300–880 K on the samples in He atmosphere. Power factor (PF) was calculated based on the measured σ and S values. The Hall carrier concentrations and mobilities were calculated using the Hall-Van der Pauw measurement system (HMS5300, Ecopia) under a 0.548 T magnetic field. The κ_{tot} values of each sample were calculated from its sample density (ρ_s), heat capacity (C_p), and thermal diffusivity (α). ρ_s was used as theoretical densities for $ReSe_2$ and Re_2Te_5. C_p, as presented in Table 1, was measured using a differential scanning calorimeter (DSC8000, Perkin Elmer). Laser-flash analysis was conducted to measure α (LFA457, Netzsch). zT was evaluated based on the measured data.

First-principle DFT calculations were performed using the generalized gradient approximation with the Perdew-Burke-Ernzerhof functional and the projector augmented plane-wave method implemented in the Vienna Ab initio Simulation program code [31–33]. The 5d/6s electrons of Re, the 4s/4p electrons of Se, and the 5s/5p electrons of Te were used as valence electrons. The plan-wave-basis cut-off energy was set to 600 eV. Self-consistency was carried out using unit cells containing 12 and 84 atoms, and $8 \times 8 \times 8$ and $4 \times 4 \times 4$ k-point meshes were used for the structural relaxation and the electronic structure calculation of $ReSe_2$ and Re_2Te_5, respectively. A van der Waals correction was included using the DFT-D3 method with Becke-Johnson rational damping [34, 35]. Structural relaxation was performed until the Hellmann-Feynman forces were less than 1×10^{-3} eV A^{-1}. The atomic positions of the relaxed structures are provided in Table S1 in Supporting Materials.

The transport properties of $ReSe_2$ and Re_2Te_5 were estimated using the Shankland-Koelling-Wood interpolation as implemented in the BoltzTraP2 code [36, 37]. First, the band structures obtained by DFT calculations were interpolated using the extended Shankland algorithm [38–40]. Next, the Onsager transport coefficients were determined using the linearized Boltzmann transport equation based on the rigid-band approximation [35]. For the calculation of the transport properties, dense $12 \times 12 \times 12$ and $6 \times 6 \times 6$ k-point meshes were used for $ReSe_2$ and Re_2Te_5, respectively.

3. Results and Discussions

Figures 1(a) and 1(c) depict the triclinic (space group: P1[2]) and orthorhombic (space group: Pbca [61]) crystal structures of $ReSe_2$ and Re_2Te_5, respectively. Figures 1(b) and

Table 1: Experimental and calculated lattice parameters of the $ReSe_2$ and Re_2Te_5.

		a (Å)	b (Å)	c (Å)	Volume (Å^3)
$ReSe_2$	Exp.	6.7211	6.6405	6.7386	249.973
	Calc.	6.7870	6.6169	6.7394	245.165
Re_2Te_5	Exp.	12.9762	12.9734	14.1738	2386.095
	Calc.	13.5152	13.4397	14.4784	2629.847

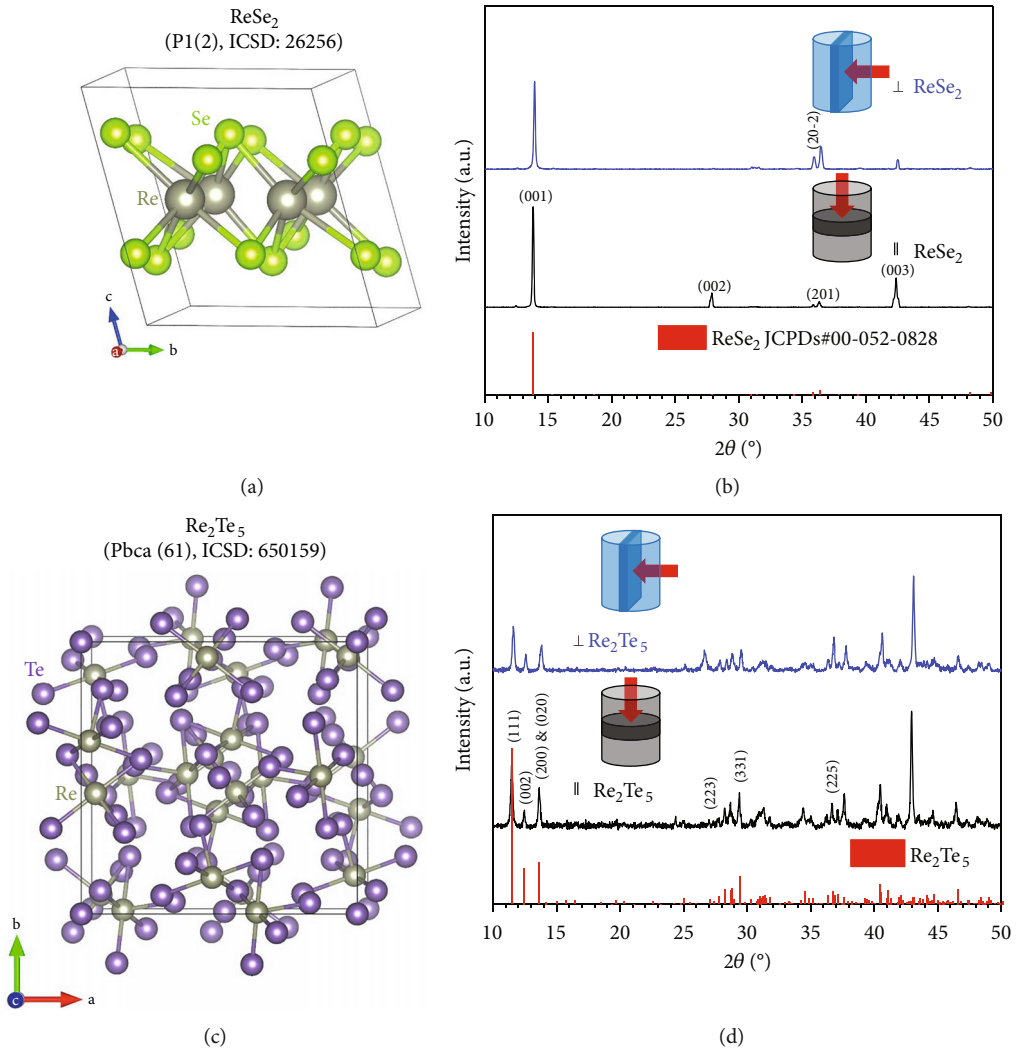

Figure 1: (a, c) Crystal structure of the (a) $ReSe_2$ and (c) Re_2Te_5, respectively. (b, d) XRD patterns of the (b) $ReSe_2$ and (d) Re_2Te_5 samples.

1(d) show XRD patterns of the $ReSe_2$ and Re_2Te_5 polycrystalline bulk samples at the 2θ range from 10° to 50°. In addition, to consider anisotropy for the samples, the measurements were performed along the directions perpendicular (⊥) and parallel (∥) to the sintering pressure direction. From the measured XRD patterns, it was observed that $ReSe_2$ and Re_2Te_5 have a single triclinic phase and a single orthorhombic phase without impurity, respectively. The lattice parameters are presented in Table 1 with the calculated lattice parameter by DFT calculation. The lattice parameters derived from the experiment were matched to those of JCPDS within an error less than 0.3%. In addition, the lattice parameters were similar with the calculated lattice parameters, while it is commonly known that the calculated lattice parameters by first-principle DFT had a larger value than those of the experimental data.

Figure 2 shows the measured thermoelectric transport properties for the $ReSe_2$ and Re_2Te_5 according to measurement directions. $ReSe_2$ and Re_2Te_5 demonstrated semiconductor transport behavior. As shown in Figures 2(a) and

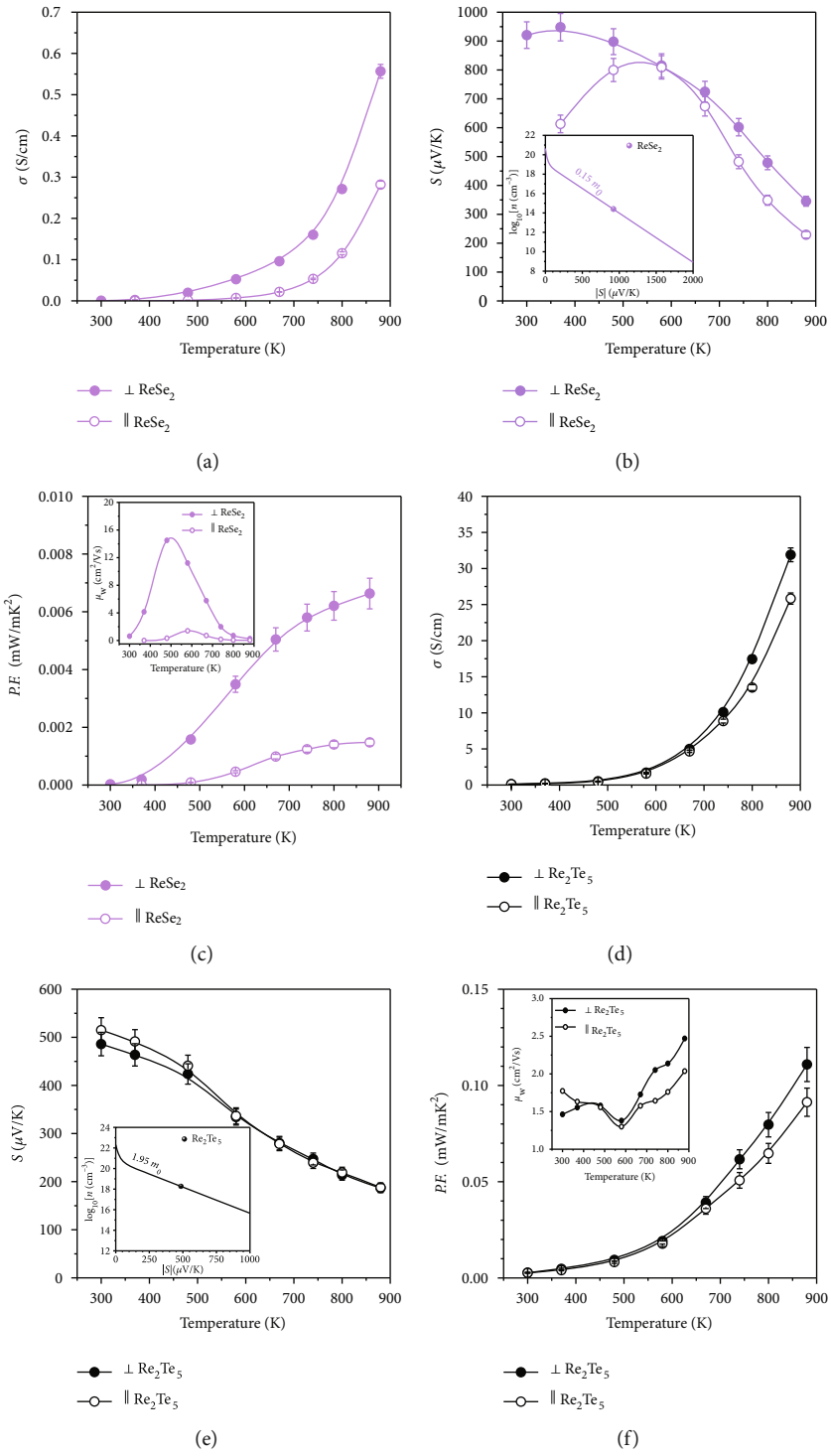

FIGURE 2: (a, d) Electrical conductivities, (b, e) Seebeck coefficients, and (c, f) power factors as a function of temperature for (a, b, c) $ReSe_2$ and (d, e, f) Re_2Te_5. Insets of (b) and (e) show common logarithmic carrier concentration as a function of absolute Seebeck coefficient, and insets of (c) and (f) show weighted mobilities.

2(d), the σ of $\perp ReSe_2$ and $\parallel ReSe_2$ are 0.0021 and 7.12×10^{-5} S/cm at 370 K, respectively, and $\perp Re_2Te_5$ and $\parallel Re_2Te_5$ are 0.12 and 0.10 S/cm at 300 K, respectively. σ of $\perp ReSe_2$ ($\parallel ReSe_2$) and $\perp Re_2Te_5$ ($\parallel Re_2Te_5$) gradually increased to 0.56 (0.28) and 32 (25.8) S/cm at 880 K, respectively. In the case of $ReSe_2$, the *ab*-axis was superior to *c*-axis; this is typical in the transport properties of a general layered structure material. Meanwhile, Re_2Te_5 did not differ significantly between the two directions. The maximum S of the $ReSe_2$ in Figure 2(b) was 948 μV/K at 370 K, which was measured

in ⊥ direction. However, in the case of Re_2Te_5 shown in Figure 2(e), $\|S$ at 300 K has a maximum value of 515 μV/K. Consequently, the calculated PF shows a maximum value in the ⊥ direction in both cases. The maximum PF values for the $ReSe_2$ and Re_2Te_5 were 0.0066 and 0.11 mW/mK^2, respectively.

Table 2 indicates the results of the Hall measurement and $m_d{}^*$ at room temperature. As presented, the large difference in σ is caused mainly by the fact that n_H of Re_2Te_5 is 10^4 times larger than the n_H of $ReSe_2$ (n_H denotes hole concentration). The $m_d{}^*$, which was calculated using Equation (1) [38], for $ReSe_2$ and Re_2Te_5, was 0.154 and 1.97 m_0 (m_0 is the rest mass of an electron), respectively. The fact that the n_H of $ReSe_2$ is significantly low is also the reason why the $m_d{}^*$ of the $ReSe_2$ is smaller than Re_2Te_5 by a factor of 12 despite its S being higher than that of Re_2Te_5. Furthermore, $\log_{10}(n)$ as function of ⊥S at 300 K was plotted for the $ReSe_2$ and Re_2Te_5 into insets of Figures 2(b) and 2(e).

$$\log_{10}\left(\frac{m_d^* T}{300}\right) = \frac{2}{3}\log_{10}(n) - \frac{2}{3}20.3 - \left[(0.00508 \times |S|) + \left(1.58 \times 0.967^{|S|}\right)\right]. \quad (1)$$

Commonly, $m_d{}^*$ was estimated using Equation (2). However, because the $m_d{}^*$ is only accurate when S is lower than 137 μV K^{-1} [41], using Equation (2) for $ReSe_2$ and Re_2Te_5 ($S > 500\ \mu$V K^{-1}) is not appropriate. Therefore, Equation (1), which is accurate for all degeneracy, was used instead.

$$S = \frac{8\pi^2 k_B^2}{3eh^2} m_d^* T\left(\frac{\pi}{3n}\right)^{2/3}. \quad (2)$$

Meanwhile, according to the measuring direction, the ⊥μ_H and $\|\mu$H values of layered $ReSe_2$ were 3.12 and 0.251 cm^2/Vs, respectively. The ⊥μ_H and $\|\mu$H values of Re_2Te_5 were confirmed as 0.308 and 0.273 cm^2/Vs, respectively.

Insets of Figures 2(c) and 2(f) are results that calculated weighted mobilities μ_w as a function of the temperature for the $ReSe_2$ and Re_2Te_5. The μ_w values were calculated from the measured σ and S; μ_w can be obtained via a simple analytical expression, wherein the exact Drude-Sommerfeld free-electron model is approximated using Equation (3) for $|S| > 20\ \mu$V/K [42].

$$\mu_w = \frac{3h^3\sigma}{8\pi e(2m_e kT)^{3/2}}\left[\frac{\exp\left[(|S|/(k/e)) - 2\right]}{1 + \exp\left[-5((|S|/(k/e)) - 1)\right]} + \frac{3/\pi^2|S|/(k/e)}{1 + \exp\left[5((|S|/(k/e)) - 1)\right]}\right], \quad (3)$$

where m_e is the mass of an electron. μ_w is proportional to the maximum PF that a sample can reach when n_H is optimized. Therefore, μ_w of $ReSe_2$ shows as significant difference as in PF with regard to the direction. However, unlike PF, maximum values of these were observed at 480 K (14.5 cm^2/Vs, ⊥μ_w) and at 580 K (1.40 cm^2/Vs, $\|\mu$w), respectively. While the difference between ⊥μ_w and $\|\mu$w of $ReSe_2$ decreases for temperatures higher than 480 K, the difference between corresponding PF increases for all temperatures. The large difference in PF observed at 880 K despite the small difference in ⊥μ_w and $\|\mu$w suggests that the $\|n$H of $ReSe_2$ is rapidly shifting away from the optimal $\|n$H. In the case of Re_2Te_5, μ_w values about the two directions were 2.47 and 2.036 cm^2/Vs, respectively. This is similar to the PF trend at 880 K.

Figures 3(a) and 3(b) show the temperature dependence of the S and σ/τ (τ: relaxation time) values for $ReSe_2$ and Re_2Te_5, respectively. For this calculation, we adopt the n_H values of 2.55×10^{14} cm^{-3} for $ReSe_2$ and 1.87×10^{18} cm^{-3} for Re_2Te_5, which are obtained by the Hall effect measurements at 300 K (see Table 2). Both compounds exhibit similar behavior; i.e., the S value decreases as temperature increases, whereas the σ/τ (τ: relaxation time) value is increased with the increase of temperature. Such trends are in good agreement with the experimental observations (Figures 2(a), 2(b), 2(d), and 2(e)), indicating that our calculational approach is suitable for the present systems. It is noted that there are distinct differences in the transport properties between $ReSe_2$ and Re_2Te_5: (i) the σ/τ values of Re_2Te_5 are higher than that of $ReSe_2$ throughout the whole temperature range, and (ii) the maximum S value of $ReSe_2$ (~1293 μV K^{-1} at 330 K) is about two times higher than that of Re_2Te_5 (~601 μV K^{-1} at 500 K).

We also calculated the doping dependence of the S and σ/τ (τ: relaxation time) values for both compounds (Figures 3(c) and 3(d)). The calculated S values are 1330 μV/K for $ReSe_2$ and 594 μV/K for Re_2Te_5 when the n_H values are 2.55×10^{14} cm^{-3} and 1.87×10^{18} cm^{-3}, respectively. These S values reasonably agree with the experimental data (see Table 2 and Figures 2(b), 2(c), and 2(e)) but are slightly overestimated. When the n_H increases, the S values of both compounds decrease, whereas the σ/τ values sharply increase. As a result, the $\sigma S^2/\tau$ values, which are directly correlated with the PF, increase rapidly at the higher n_H until the maximum $\sigma S^2/\tau$ is reached. This result indicates that the higher PF of Re_2Te_5 compared with that of $ReSe_2$ in our experimental observation (Figures 2(c) and 2(f)) mainly originates from the ~10^4 times higher n_H of Re_2Te_5, rather than other parameters such as maximum PF. The optimal n_H values to achieve the maximum PF can be estimated as ~10^{20} cm^{-3} for both compounds, suggesting that the thermoelectric performance can be further improved by introducing additional hole carriers into $ReSe_2$ and Re_2Te_5.

The electronic band structures and density of states (DOS) for $ReSe_2$ and Re_2Te_5 are calculated to elucidate the correlation between the thermoelectric properties and the electronic structure. The calculated band structures and DOS for $ReSe_2$ and Re_2Te_5 are shown in Figures 3(e) and 3(f), respectively. Both compounds have finite band gaps with values of ~0.9 eV and ~0.7 eV, consistent with the experimentally observed semiconducting transport behavior (Figures 2(a) and 2(d)). By comparing the electronic band structures of $ReSe_2$ and Re_2Te_5, it was found that Re_2Te_5 has a more complex band structure near the valence band

Table 2: Hall measurement results, density of state effective mass, and heat capacity for $ReSe_2$ and Re_2Te_5 at room temperature.

Samples	n_H (cm^{-3})	$\perp\mu_H$ (cm^2/Vs)	$\|\|\mu H$ (cm^2/Vs)	$m_d{}^*$ (m_0)	C_p (J/gK)
$ReSe_2$	2.55×10^{14}	3.12	0.251	0.154	0.212
Re_2Te_5	1.87×10^{18}	0.308	0.273	1.97	0.157

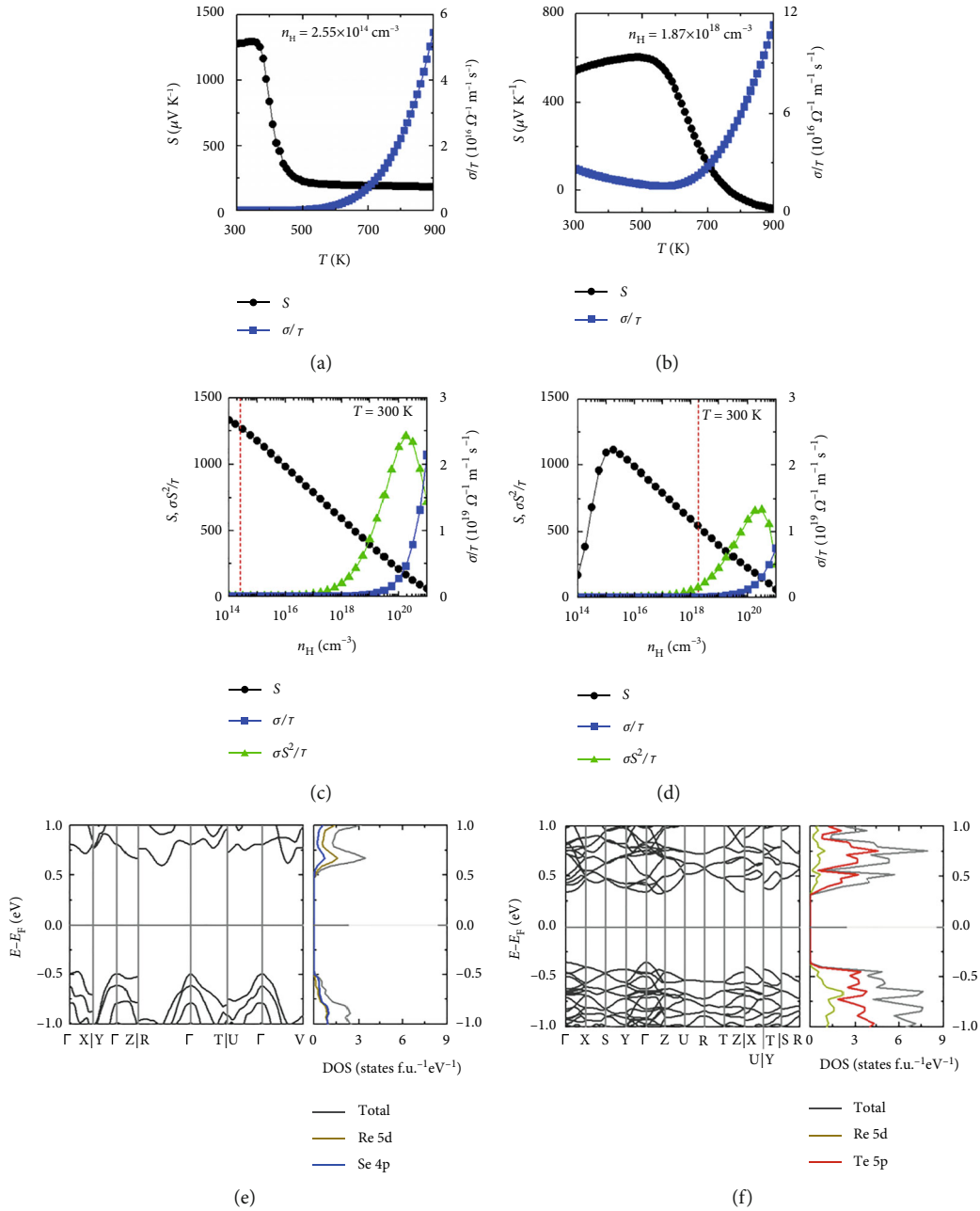

Figure 3: Calculated transport properties and electronic structures. (a, b) Temperature (T) dependence of S and σ/τ for $ReSe_2$ (a) and Re_2Te_5 (b). (c, d) n_H dependence of S, σ/τ, and $\sigma S^2/\tau$ for $ReSe_2$ (c) and Re_2Te_5 (d). Dashed red lines indicate the n_H values of 2.55×10^{14} cm^{-3} for $ReSe_2$ and 1.87×10^{18} cm^{-3} for Re_2Te_5. (e, f) Band structures and total/projected DOSs of $ReSe_2$ (e) and Re_2Te_5 (f).

maximum as compared with that of $ReSe_2$. Such higher band degeneracy facilitates the substantial enhancement of the DOS near the valence band maximum, which mainly consists of Te 5p orbitals (right panel in Figure 3(f)). The high band degeneracy and effective DOS near the valence band maximum are beneficial to achieve a higher power factor in the p-type doping regime [43]. This distinct difference in electronic structures can be understood by comparing their different crystal structure; i.e., the Re cations in $ReSe_2$ are only bound to the nearby Se anions (Figure 1(a)),

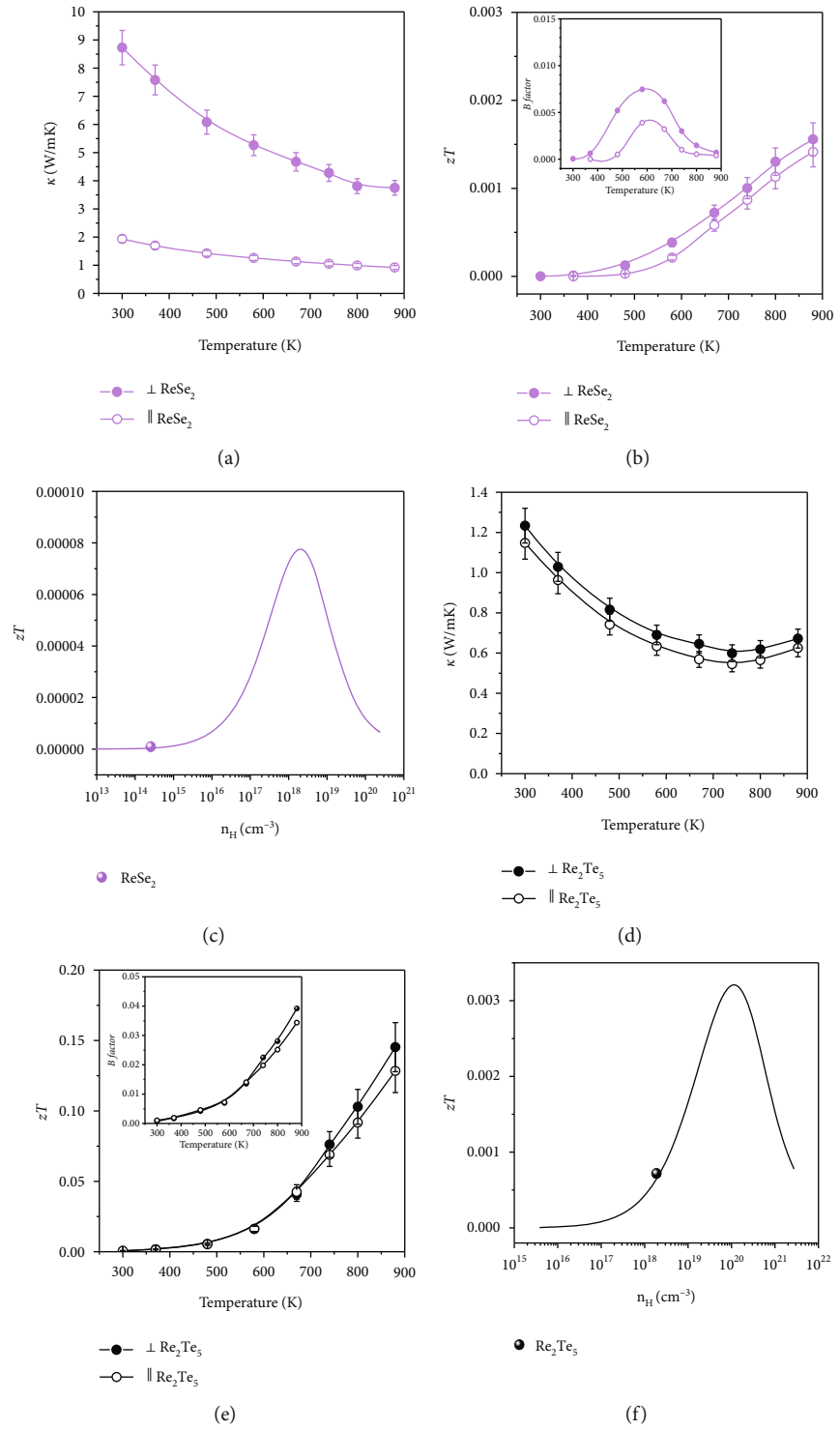

FIGURE 4: (a, d) κ_{tot} and (b, e) zT as a function of the temperature for (a, b) $ReSe_2$ and (d, e) Re_2Te_5. Insets of (c) and (f) show calculated B factor. (c, f) Predicted zT of the (c) $ReSe_2$ and (f) Re_2Te_5 at 300 K calculated based on the single parabolic band model as a function of n_H.

whereas the crystal structure of Re_2Te_5 consists of the mixture of the homopolar Te–Te bonds and heteropolar Re–Te bonds (Figure 1(c)), inducing a complex electronic structure.

Figures 4(a) and 4(d) show calculated κ of $ReSe_2$ and Re_2Te_5. κ values of $ReSe_2$ were gradually decreased in both $\perp$ and $\parallel$ directions as the temperature changed. $\perp\kappa$ and $\|\kappa$ were 1.93 and 8.73 W/mK at 300 K, respectively, which are quite large. The large difference between two directions is due to the layered structure. The $\perp\kappa$ and $\|\kappa$ were gradually decreased to 0.920 and 3.75 W/mK at 880 K. For Re_2Te_5, which has the complex crystal structure, the κ value was in

the range between 0.62 and 1.23 W/mK. The κ of Re_2Te_5 can be further reduced by possible doping in 4 large vacancies in the unit cell, which can cause rattling effect [27].

Figures 4(b) and 4(e) show evaluated zT as a function of temperature, while the insets show a dimensionless thermoelectric quality factor B for $ReSe_2$ and Re_2Te_5. The maximum zT values of $ReSe_2$ and Re_2Te_5 were 0.0016 and 0.145, respectively, in the $\perp$ direction at 880 K. The zT of $ReSe_2$ is very low due to low σ and high κ, which are not adequate for the good thermoelectric materials. Meanwhile, the relatively high zT of 0.145 in Re_2Te_5 is originated from the acceptable PF higher than 0.1 mW/mK^2 and the low-enough κ smaller than 1.0 W/mK.

The dimensionless thermoelectric quality factor B [39] (the insets of Figures 4(b) and 4(e)) is another measure of thermoelectric performance of materials, which can be obtained using the following [39]:

$$B = \left(\frac{k}{e}\right)^2 \frac{8\pi e(2m_e kT)^{3/2}}{3h^3} \bullet \frac{\mu_w}{\kappa_{latt}} T. \quad (4)$$

B of $ReSe_2$ is quite low and shows similar trend to μ_w, which shows the maximum values at midtemperature. B of Re_2Se_5 shows the maximum value of 0.039 at 880 K.

Figures 4(c) and 4(f) depict the plot of the experimental $\perp zT$ of $ReSe_2$ and Re_2Te_5 (in symbol) and the calculated $\perp zT$ of $ReSe_2$ and Re_2Te_5 (in line) as a function of n_H at 300 K using a single parabolic band (SPB) model under acoustic phonon scattering assumption:

$$zT = \frac{B((2F_1(\eta)/F_0(\eta)) - \eta)^2 F_0(\eta)}{1 + B\left[(3F_2(\eta)/F_0(\eta)) - (2F_1(\eta)/F_0(\eta))^2\right] F_0(\eta)}, \quad (5)$$

where $F_x(\eta)$ (η is the reduced electrochemical potential) is the Fermi integral of order x.

$$F_x(\eta) = \int_0^\infty \frac{\varepsilon^x d\varepsilon}{1 + e^{(\varepsilon - \eta)}}. \quad (6)$$

According to the SPB model, both $\perp zT$ of $ReSe_2$ and Re_2Te_5 can be significantly improved once n_H is optimized. For example, the maximum $\perp zT$ at 300 K predicted for $ReSe_2$ and Re_2Te_5 are 9.3×10^{-4} and 3.2×10^{-3} at 300 K, respectively. Based on appropriate n_H tuning, $\perp zT$ of $ReSe_2$ and Re_2Te_5 can be improved by more than a factor of 83 ($9.3 \times 10^{-7} \longrightarrow 7.8 \times 10^{-5}$) and 4 ($7.2 \times 10^{-4} \longrightarrow 3.2 \times 10^{-3}$), respectively. The optimization of n_H by proper doping in Re_2Te_5 by various strategies, including cation/anion doping and impurity control, may further increase the zT.

In this study, the electrical, thermal, and thermoelectric transport properties of $ReSe_2$ and Re_2Te_5 polycrystalline alloys are systematically investigated. The maximum power factor values for the $ReSe_2$ and Re_2Te_5 were measured 0.0066 and 0.11 mW/mK^2 at 880 K, respectively. The differences in electronic transport properties between $ReSe_2$ and Re_2Te_5 were verified with density of state and electronic dispersion calculated from first-principle density functional theory. Thermal conductivity of layered $ReSe_2$ at room temperature was between 1.93 and 8.73 W/mK according to the measuring direction, which of both are relatively high. For Re_2Te_5 with the complex crystal structure, the thermal conductivity was low in the range between 0.62 and 1.23 W/mK at room temperature. As a result, the maximum thermoelectric figure of merit zT values of $ReSe_2$ was quite low as 0.0016 at 880 K due to very low power factor and high thermal conductivity. On the other hand, the relatively high zT of 0.145 in Re_2Te_5 is seen due to the decent power factor value and the low thermal conductivity. Indeed, adequate doping can enhance the zT of Re_2Te_5 by further enhancing the power factor by controlling the carrier concentration and reducing the thermal conductivity by filling the 4 large vacancies in the unit cell by rattling effect.

Data Availability

Data are available upon request.

Conflicts of Interest

There is no conflict of interest.

Authors' Contributions

Joonho Bang, Okmin Park, and Hyun-Sik Kim contributed equally to this work.

Acknowledgments

This research was supported by Nano·Material Technology Development Program through National Research Foundation of Korea (NRF) funded by the Ministry of Science and ICT (2022M3H4A1A04076667).

Supplementary Materials

Additional supporting information may be found in the online version of the article at the publisher's website. The atomic positions of the relaxed structures of $ReSe_2$ and Re_2Te_5 are provided in Table S1 in Supporting Materials. *(Supplementary Materials)*

References

[1] X. Huang, Z. Zeng, and H. Zhang, "Metal dichalcogenide nanosheets: preparation, properties and applications," *Chemical Society Reviews*, vol. 42, no. 5, pp. 1934–1946, 2013.

[2] Y. Wang, Y. Zhao, X. Ding, and L. Qiao, "Recent advances in the electrochemistry of layered post-transition metal chalcogenide nanomaterials for hydrogen evolution reaction," *Journal of Energy Chemistry*, vol. 60, pp. 451–479, 2021.

[3] D. Aldakov, A. Lefrançois, and P. Reiss, "Ternary and quaternary metal chalcogenide nanocrystals: synthesis, properties and applications," *Journal of Materials Chemistry C*, vol. 1, no. 24, pp. 3756–3776, 2013.

[4] M. M. Alsalama, H. Hamoudi, A. Abdala, Z. K. Ghouri, and K. M. Youssef, "Enhancement of thermoelectric properties of layered chalcogenide materials," *Reviews on Advanced Materials Science*, vol. 59, no. 1, pp. 371–378, 2020.

[5] A. Maignan, E. Guilmeau, F. Gascoin, Y. Bréard, and V. Hardy, "Revisiting some chalcogenides for thermoelectricity," *Science and Technology of Advanced Materials*, vol. 13, no. 5, article 053003, 2012.

[6] R. Dutt, J. Bhattacharya, and A. Chakrabarti, "Investigation of mechanical, lattice dynamical, electronic and thermoelectric properties of half heusler chalcogenides: a DFT study," *Journal of Physics and Chemistry of Solids*, vol. 167, article 110704, 2022.

[7] X. Yan, B. Poudel, Y. Ma et al., "Experimental studies on anisotropic thermoelectric properties and structures of n-type $Bi_2Te_{2.7}Se_{0.3}$," *Nano Letters*, vol. 10, no. 9, pp. 3373–3378, 2010.

[8] P. K. Nguyen, K. H. Lee, J. Moon et al., "Spark erosion: a high production rate method for producing $Bi_{0.5}Sb_{1.5}Te_3$ nanoparticles with enhanced thermoelectric performance," *Nanotechnology*, vol. 23, no. 41, article 415604, 2012.

[9] L. Hu, T. Zhu, X. Liu, and X. Zhao, "Point defect engineering of high-performance bismuth-telluride-based thermoelectric materials," *Advanced Functional Materials*, vol. 24, no. 33, pp. 5211–5218, 2014.

[10] K. H. Lee, M. W. Oh, H. S. Kim et al., "Enhanced thermoelectric transport properties of n-type InSe due to the emergence of the flat band by Si doping," *Inorganic Chemistry Frontiers*, vol. 6, no. 6, pp. 1475–1481, 2019.

[11] J.-S. Rhyee, K. H. Lee, S. M. Lee et al., "Peierls distortion as a route to high thermoelectric performance in In4Se3-δ crystals," *Nature*, vol. 459, no. 7249, pp. 965–968, 2009.

[12] S.-i. Kim, J. Bang, J. An et al., "Effect of Br substitution on thermoelectric transport properties in layered $SnSe_2$," *Journal of Alloys and Compounds*, vol. 868, article 159161, 2021.

[13] J. Bang, H.-S. Kim, D. H. Kim, S. W. Lee, O. Park, and S.-i. Kim, "Phase formation behavior and electronic transport properties of $HfSe_2$-$HfTe_2$ solid solution system," *Journal of Alloys and Compounds*, vol. 920, article 166028, 2022.

[14] Y. Kim, W. J. Woo, D. Kim et al., "Atomic-layer-deposition-based 2D transition metal chalcogenides: synthesis, modulation, and applications," *Advanced Materials*, vol. 33, no. 47, article 2005907, 2021.

[15] C. Han, Q. Sun, Z. Li, and S. X. Dou, "Thermoelectric enhancement of different kinds of metal chalcogenides," *Advanced Energy Materials*, vol. 6, no. 15, article 1600498, 2016.

[16] S. Kumar and U. Schwingenschlögl, "Thermoelectric response of bulk and monolayer MoSe2and WSe_2," *Chemistry of Materials*, vol. 27, no. 4, pp. 1278–1284, 2015.

[17] M. Hafeez, L. Gan, H. Li, Y. Ma, and T. Zhai, "Chemical vapor deposition synthesis of ultrathin hexagonal $ReSe_2$ flakes for anisotropic Raman property and optoelectronic application," *Advanced Materials*, vol. 28, no. 37, pp. 8296–8301, 2016.

[18] S. Yang, C. Wang, H. Sahin et al., "Tuning the optical, magnetic, and electrical properties of $ReSe_2$ by nanoscale strain engineering," *Nano Letters*, vol. 15, no. 3, pp. 1660–1666, 2015.

[19] E. Zhang, P. Wang, Z. Li et al., "Tunable ambipolar polarization-sensitive photodetectors based on high-anisotropy $ReSe_2$ nanosheets," *ACS Nano*, vol. 10, no. 8, pp. 8067–8077, 2016.

[20] K. K. Tiong, C. H. Ho, and Y. S. Huang, "The electrical transport properties of ReS_2 and $ReSe_2$ layered crystals," *Solid State Communications*, vol. 111, no. 11, pp. 635–640, 1999.

[21] M. Hafeez, L. Gan, A. Saleem Bhatti, and T. Zhai, "Rhenium dichalcogenides (ReX_2, X = S or Se): an emerging class of TMDs family," *Materials Chemistry Frontiers*, vol. 1, no. 10, pp. 1917–1932, 2017.

[22] D. Wolverson, S. Crampin, A. S. Kazemi, A. Ilie, and S. J. Bending, "Raman spectra of monolayer, few-layer, and bulk $ReSe_2$: an anisotropic layered semiconductor," *ACS Nano*, vol. 8, no. 11, pp. 11154–11164, 2014.

[23] F. Wang, J. Wang, S. Guo, J. Zhang, Z. Hu, and J. Chu, "Tuning coupling behavior of stacked heterostructures based on MoS_2, WS_2, and WSe_2," *Scientific Reports*, vol. 7, no. 1, pp. 1–10, 2017.

[24] M. M. A. Mahmoud and D. P. Joubert, "First principles study of the structural, stability properties and lattice thermal conductivity of bulk $ReSe_2$," *Materials Today: Proceedings*, vol. 5, no. 4, pp. 10424–10430, 2018.

[25] S. G. Kozlova, S. P. Gabuda, and V. V. Terskikh, "^{125}Te NMR tomography of [Re_6] cluster in Re_6Te_{15} and related cluster compounds," *Solid State Nuclear Magnetic Resonance*, vol. 25, no. 1-3, pp. 72–75, 2004.

[26] C. Godart, A. P. Gonçalves, E. B. Lopes, and B. Villeroy, *Properties and Applications of Thermoelectric Materials*, Springer, 2009.

[27] T. Caillat and J.-P. Fleurial, "New low thermal conductivity materials for thermoelectric applications," *XVI ICT '97. Proceedings ICT'97. 16th International Conference on Thermoelectrics*, 1997, pp. 446–453, Institute of Electrical and Electronics Engineers, New York, Dresden, Germany, August 1997.

[28] T. Caillat, S. Chung, J. P. Fleurial, G. J. Snyder, and A. Borshchevsky, "17th International Conference on Thermoelectrics," in *Seventeenth International Conference on Thermoelectrics. Proceedings ICT98 (Cat. No.98TH8365)*, pp. i–ii, Nagoya, Japan, 1998.

[29] S. Kilibarda-Dalafave and J. Ziegler, "Seebeck coefficient and electrical resistivity in Re6Te15–xSex at room temperature," *Journal of Materials Science Letters*, vol. 17, no. 17, pp. 1463–1465, 1998.

[30] T. Caillat, J.-P. Fleurial, and G. J. Snyder, "Potential of Chevrel phases for thermoelectric applications," *Solid State Sciences*, vol. 1, no. 7-8, pp. 535–544, 1999.

[31] G. Kresse and J. Furthmuller, "Efficient iterative schemes for*ab initio*total-energy calculations using a plane-wave basis set," *Physical Review B*, vol. 54, no. 16, pp. 11169–11186, 1996.

[32] P. E. Blöchl, "Projector augmented-wave method," *Physical Review B*, vol. 50, no. 24, pp. 17953–17979, 1994.

[33] J. P. Perdew, K. Burke, and M. Ernzerhof, "Generalized gradient approximation made simple," *Physical Review Letters*, vol. 77, no. 18, pp. 3865–3868, 1996.

[34] S. Grimme, J. Antony, S. Ehrlich, and H. Krieg, "A consistent and accurate ab initio parametrization of density functional dispersion correction (DFT-D) for the 94 elements H-Pu," *The Journal of Chemical Physics*, vol. 132, no. 15, article 154104, 2010.

[35] S. Grimme, S. Ehrlich, and L. Goerigk, "Effect of the damping function in dispersion corrected density functional theory," *Journal of Computational Chemistry*, vol. 32, no. 7, pp. 1456–1465, 2011.

[36] W. E. Pickett, H. Krakauer, and P. B. Allen, "Smooth Fourier interpolation of periodic functions," *Physical Review B: Condensed Matter and Materials Physics*, vol. 38, no. 4, pp. 2721–2726, 1988.

[37] G. K. H. Madsen, J. Carrete, and M. J. Verstraete, "BoltzTraP2, a program for interpolating band structures and calculating

semi-classical transport coefficients," *Computer Physics Communications*, vol. 231, pp. 140–145, 2018.

[38] R. N. Euwema, D. J. Stukel, T. C. Collins, J. S. DeWitt, and D. G. Shankland, "Crystalline interpolation with applications to Brillouin-zone averages and energy-band interpolation," *Physics Review*, vol. 178, no. 3, pp. 1419–1423, 1969.

[39] D. G. Shankland, "Fourier transformation by smooth interpolation," *International Journal of Quantum Chemistry*, vol. 5, no. S5, pp. 497–500, 1971.

[40] D. D. Koelling and J. H. Wood, "On the interpolation of eigenvalues and a resultant integration scheme," *Journal of Computational Physics*, vol. 67, no. 2, pp. 253–262, 1986.

[41] K. H. Lee, S. I. Kim, J. C. Lim, J. Y. Cho, H. Yang, and H. S. Kim, "Approach to determine the density-of-states effective mass with carrier concentration-dependent seebeck coefficient," *Advanced Functional Materials*, vol. 32, no. 33, article 2203852, 2022.

[42] G. J. Snyder, A. H. Snyder, M. Wood, R. Gurunathan, B. H. Snyder, and C. Niu, "Weighted mobility," *Advanced Materials*, vol. 32, no. 25, article 2001537, 2020.

[43] N. Wang, M. Li, H. Xiao et al., "Band degeneracy enhanced thermoelectric performance in layered oxyselenides by first-principles calculations," *Npj Computational Materials*, vol. 7, no. 1, pp. 1–13, 2021.